Mechanical behaviour of additively manufactured elastomeric pre-buckled honeycombs under quasi-static and impact loading

Rhosslyn Adams [a], Scott Townsend [a], Shwe Soe [b], Peter Theobald [a],*

[a] *School of Engineering, Cardiff University, UK*
[b] *Department of Engineering, Design and Mathematics, University of the West of England, UK*

HIGHLIGHTS

- Elastomeric pre-buckled circular honeycombs were additively manufactured and tested under static and dynamic loading.
- Variable mechanical behaviour can be achieved through informed selection of pre-buckled design feature's aspect ratio.
- Periodic boundary condition finite element represents a method to accurate and computationally efficient simulation.
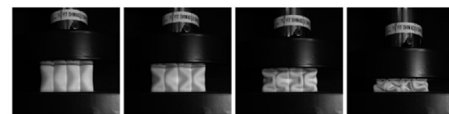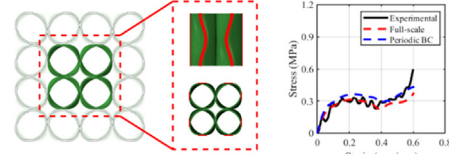
GRAPHICAL ABSTRACT
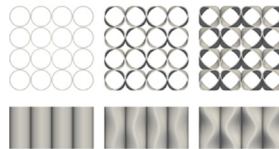
ARTICLE INFO

ABSTRACT

Selective laser sintering has been used to manufacture different structural variations of a pre-buckled circular honeycomb. The mechanical behaviour of these structures has been examined under both quasi-static and dynamic impact loading. Pre-buckled circular honeycombs with aspect ratios e = 0.8 and e = 0.6 were compared to a traditional, straight-walled honeycomb. It has been found that the mechanical behaviour of the honeycomb can be tailored to yield different mechanical responses. Principally, decreasing the aspect ratio reduced the stress at yield, as well as the total energy absorbed until densification, however, this alleviated the characteristic stress-softening response of traditional honeycombs under static and dynamic conditions. When subjected to multiple cycles of loading, a stabilised response was observed. The numerical response closely agreed with the experimental results. A simplified, periodic boundary condition model also closely agreed with the experimental results whilst alleviating computational run time by nominally 75%. The numerical full factorial parameter design sweep identified a broad range of mechanical behaviour. This represents a valuable tool to identify optimal design configurations for future impact mitigating applications.

1. Introduction

The honeycomb is a classical structure defined as an array of identical prismatic cells, nesting together to fill a plane [1]. These structures are found in nature, e.g., bee's honeycomb, as well as in man-made applications. In the latter, they are leveraged for their notable high specific stiffness [2] and therefore are the preferred design route to achieve lightweight structures with high energy absorption ability. Consequently, they are increasingly being employed in applications such as personal protective equipment,

---

* Corresponding author.
E-mail address: TheobaldPS@Cardiff.ac.uk (P. Theobald).

as an alternative to polymeric foams, e.g. expanded polystyrene (EPS) [3].

Honeycomb structures can be fabricated via expansion, corrugation, moulding and extrusion [1]; however, such methods only allow linear projections (i.e., two-and-a-half dimensions), prohibiting novel geometries. Design freedom is further constrained by limited material choice and needing flat, planar configurations. The evolution of additive manufacturing (AM) has accelerated the development of new honeycomb structures to include complex geometries such as hierarchical features [4,5], functional grading schemes [6,7], folds [8,9], hinges [10,11] as well as propagation throughout curved volumes [12,13]. Moreover, broader fabrication opportunities now exist, including material derived from composites [14,15], metal alloys [16,17], polymers [18,19] and elastomers [20].

Strategic geometry and material selection represents an effective method to tailor a honeycomb's mechanical behaviour [21,22]. For example, *Bates et. al* reported that hexagonal honeycombs manufactured from thermoplastic polyurethane achieved recoverable and repeatable behaviour under cyclic compression [23]. Furthermore, the behaviour of these structures could be tailored by changing the unit cell geometry [24]. *Park et. al* investigated personal protective equipment by leveraging additive manufacturing, demonstrating the efficacy of elastomeric honeycombs at mitigating impact loads associated with falls [25]. *Townsend et. al* investigated the energy absorption ability of elastomeric origami-inspired honeycombs [26]. Through inclusion of a pre-buckled feature (i.e., a fold), it was reported that it is feasible to retain the characteristic stiffness-to weight ratio of honeycombs, whilst removing the undesirable stress-softening phenomena. Hence, there is good potential to tune the mechanical behaviour of elastomeric pre-buckled structures for repeat, impact mitigating applications that are subject to variable, application-specific loading regimes [27] which would not otherwise be effectively mitigated by EPS foam [28]. Additive manufacturing now represents a feasible route to low volume manufacture, meaning these structures can now offer an alternative to the current state of the art.

This study aims to investigate the mechanical behaviour and energy absorption ability of various circular, pre-buckled honeycombs under static and dynamic compressive loading as an alternative to EPS foam. Moreover, these conditions will be applied to the structure for multiple loading regimes. Laser sintering of a thermoplastic polyurethane powder is adopted to fabricate the structures for experimental characterisation. Finite element simulations, including computationally efficient periodic boundary condition models, are developed and then validated by comparison to experimental data, enabling numerical parameter sweeps of the geometric design space. The outcome of this study will provide a foundation for optimising these structures for future design applications, based on specific loading regimes and acceptable performance thresholds.

2. Materials & methods

2.1. Materials

2.1.1. Honeycomb geometry

As illustrated by Fig. 1, the circular honeycomb topology unit cell is defined by geometric parameters: cell size (w), wall thickness (t), and depth (h). The pre-buckled design feature, characterised as a smooth cosine curve propagated through the z axis, is defined by geometric parameters: aspect ratio ($e = r_1/r_2$) and number of folds (f).

Computer-aided design (CAD) models were generated using an in-house software written in python code. As illustrated by Fig. 2, the honeycomb with an aspect ratio of e = 1.0 retrieves a basic circular cross-section and straight walls in the z-direction. As e reduces, the tube cross section becomes more elliptical, and the pre-buckled feature become more pronounced. As such, e controls both the ratio of side lengths in the cross section and the angle in the z-direction.

3. Selective laser sintering

Three honeycombs of 16 cells (4 × 4 array) were designed with overall dimensions 50 mm × 50 mm × 25 mm, a constant wall thickness of 0.6 mm and aspect ratios of 1.0, 0.8, and 0.6. Parts were built using selective laser sintering adopting a 0.1 mm layer thickness from Luvosint X92A-1 (Lehmann & Voss & Co; Hamburg, Germany), a thermoplastic polyurethane powder. Post-processing using pressured air remove un-sintered powder. Manufacturing was sub-contracted to a specialist third party.

3.1. Methods

3.1.1. Experimental testing

3.1.1.1. Quasi-static compression. Quasi-static uniaxial compression testing was performed with a universal mechanical tester (Zwick Z50; Ulm, Germany) as illustrated in Fig. 3. The specimen was placed between two horizontal, rigid plates fitted with a 50kN load cell; the upper platen was translated vertically at a rate of 100 mm/min, equivalent to a strain rate of 0.06/s, until a strain of 0.75 mm/mm. Force was measured using the load cell and displacement was recorded using the in-built measurement system. Engineering strain was calculated by dividing the displacement of the upper plate by the honeycomb height. Engineering stress was calculated by dividing the recorded force by the projected area of the honeycomb. A video capture system (iMetrum CAM028; Bristol, UK) was used to record the deformation mechanisms. All specimens were compressed out-of-plane, aligned with the build orientation. Three specimens of each structural design were tested for statistical analysis. All testing was performed in ambient laboratory conditions.

3.1.2. Dynamic compression

Dynamic uniaxial compression tests were performed using a twin-wire shock absorption test facility (model: 1002 MAU1006/CF/ALU; AD Engineering, Bergamo, Italy) as illustrated by Fig. 4. Each honeycomb was taped to the upper plate of the drop carriage and positioned centrally within a pre-marked area. The drop carriage, which weighed 6.1 kg in total, was then wire-guided, under free-fall, onto a steel anvil that had a 50 kN load cell positioned within it. Displacement-time information was calculated using the double integration of the acceleration-time data of the upper plate, informed by the initial velocity condition recorded by the light gate. During the impact, a high-speed video camera (Edgertronic SC1, Sanstreak Corp, USA) was used to capture the deformation mechanisms as well as validate a consistent strain rate of the upper plate. All data was recorded at 50 Hz and filtered in accordance with ISO 6487 class 1000. Engineering strain was calculated by dividing the displacement of the upper plate by the honeycomb height. Engineering stress was calculated by dividing the recorded force by the projected area of the honeycomb. Each sample was subjected to an initial impact velocity of 2.5 m/s, selected to achieve a 100/s strain rate, the upper limit of validity for the material model used in the numerical analysis. The kinetic energy of the impactor was chosen such that densification of the structure was achieved without causing a notable deviation in strain-rate throughout the compression. All specimens were compressed out-of-plane to the build orientation. Three specimens of each structural design were tested for statistical analysis. All testing was performed in ambient laboratory conditions.
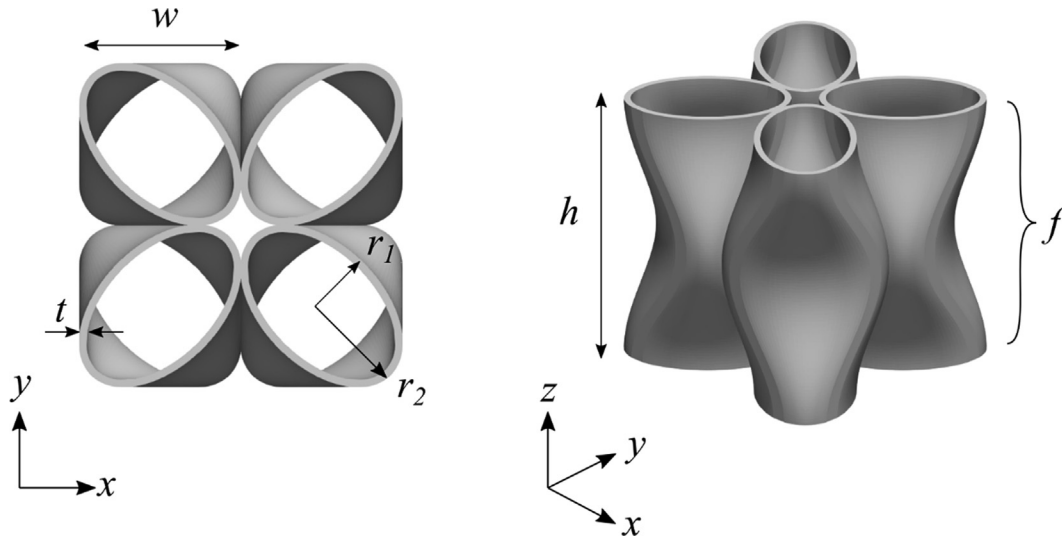
Fig. 1. Annotated circular honeycomb (2x2) with geometric parameters of the unit cell.
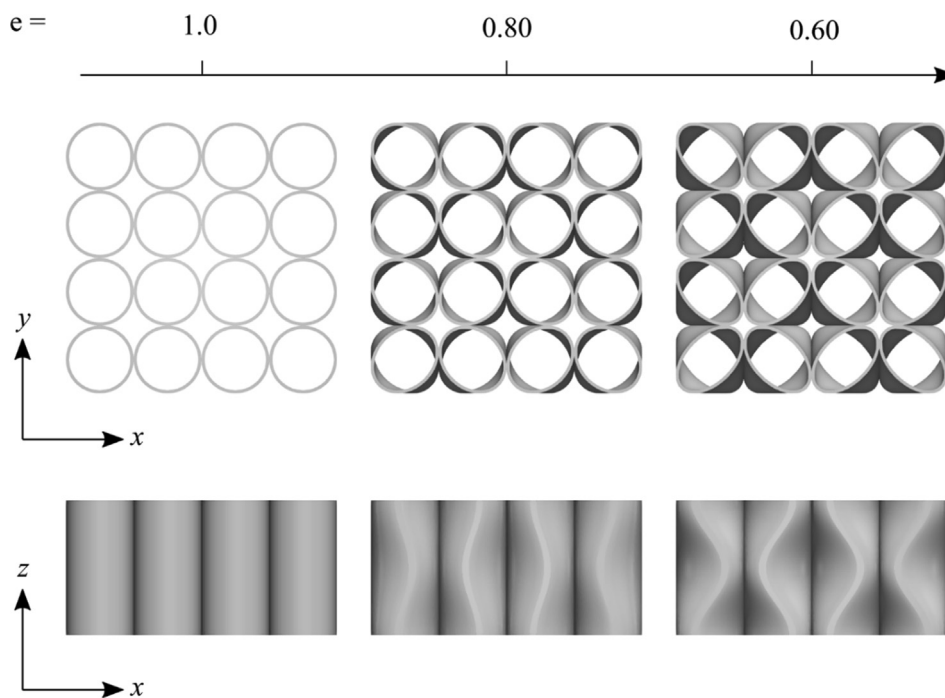

Fig 2. Variation in pre-buckled honeycomb design subject to changing aspect ratio.

3.1.3. Numerical testing

3.1.3.1. Quasi-static compression. The quasi-static compression model was constructed using finite element analysis software (Abaqus Explicit 2019; Dassault Systems, France). It is important to note that although in this investigation the quasi-static response is analysed, the explicit dynamic solver in Abaqus was utilised to access the general contact algorithm. As illustrated by Fig. 5, the honeycomb structure was positioned between two analytically rigid plates. The lower plate was assigned an encastre boundary condition, whilst the upper plate was assigned a ramp deformation boundary condition achieving a strain of 0.75 mm/mm in the z-direction. An eight-node brick element, with hexahedron shape type, reduced integration and hourglass control was utilised (C3D8R). The mesh density was selected so that there were two elements across the wall thickness to mitigate against shear locking. Mesh independence studies identified an average element size of 0.3 mm was sufficient, with a finer mesh yielding better results, however, disproportionality greater computational runtime. A global friction value of 1.0 was adopted [29]. An Ogden N5 material model was used to represent the hyperelastic behaviour, whilst Prony series was used to represent the linear viscoelastic model (material model coefficients can be found Table A2 and A3 of the appendix). Our previous work characterised Luvosint's material behaviour under uniaxial, planar and equiaxial tension, as well as single step stress relaxation characterisation. The numerical material model was validated under quasi-static and dynamic, isolated and mixed deformation testing [30]. Reaction force and displacement was extracted from a reference point at the centre of the upper plate. Strain was calculated by dividing the displacement of the upper plate by the honeycomb height. Stress was calculated by dividing the recorded force by the projected area of the honeycomb.
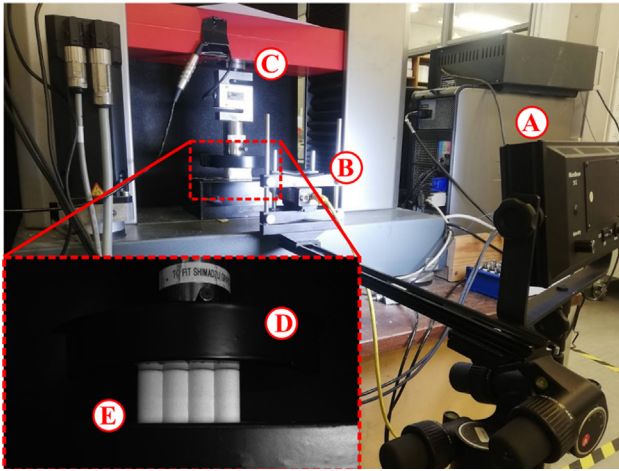
Fig. 3. Experimental test setup for quasi-static uniaxial compression including light source (A), video capture system (B), load cell (C), compressive plates (D), and honeycomb sample (E).
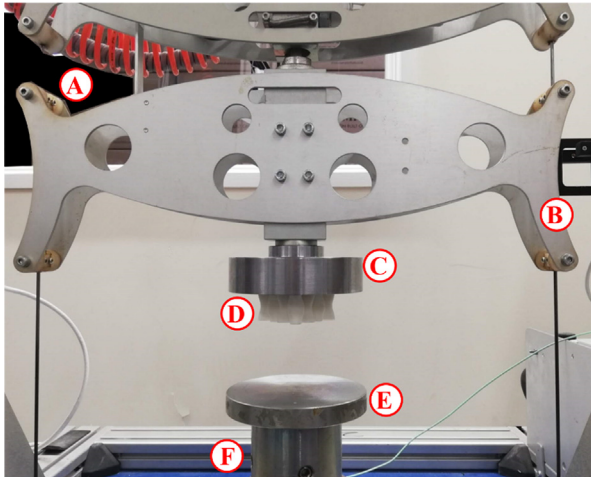

Fig. 4. Experimental test setup for dynamic uniaxial compression including carriage (A), light gate (B), impact plate (C), honeycomb sample (D), anvil (E), load cell (F).

3.1.3.2. Dynamic compression. The dynamic compression model was constructed analogous to the quasi-static model. The lower plate was assigned an encastre boundary condition, whilst the upper plate was assigned a 6.1 kg point mass and prescribed a pre-impact velocity of 2.5 m/s.
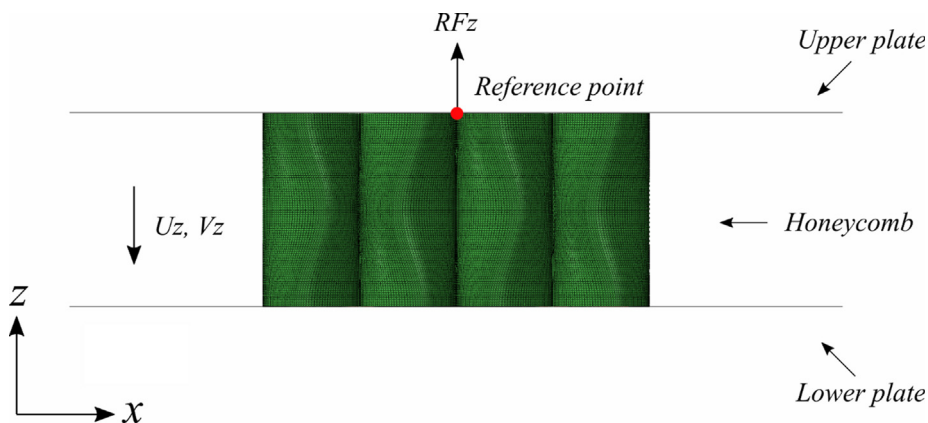
3.1.3.3. Periodic boundary condition model. In addition to the previously discussed finite element models, hereafter referred to as the full-scale models, two computationally efficient models were developed, termed periodic boundary condition (BC) models. As illustrated by Fig. 6, these were achieved by taking advantage of the symmetry in the X and Y plane and utilising zero displacement boundary conditions around the perimeter of the unit cell.

In the quasi-static model, a 2×2 honeycomb configuration was modelled with zero displacement in the X and Y axes prescribed along the perimeter nodes. The displacement conditions of the upper and lower plates were identical to the previous model. The dynamic model adopted a similar boundary condition approach. The lower plate boundary conditions remained the same, whilst the upper plate point mass was scaled by factor of 0.25, which is proportional to the kinetic energy, to account for load distribution over a quarter of the projected area.

3.1.3.4. Performance parameters. To assess the energy absorption capacity of each honeycomb variant, the following performance parameters were used: yield stress, energy absorption and absorption efficiency. Yield stress was defined as the peak load during initial yield (nominally between 0 and 0.2 mm/mm). Energy
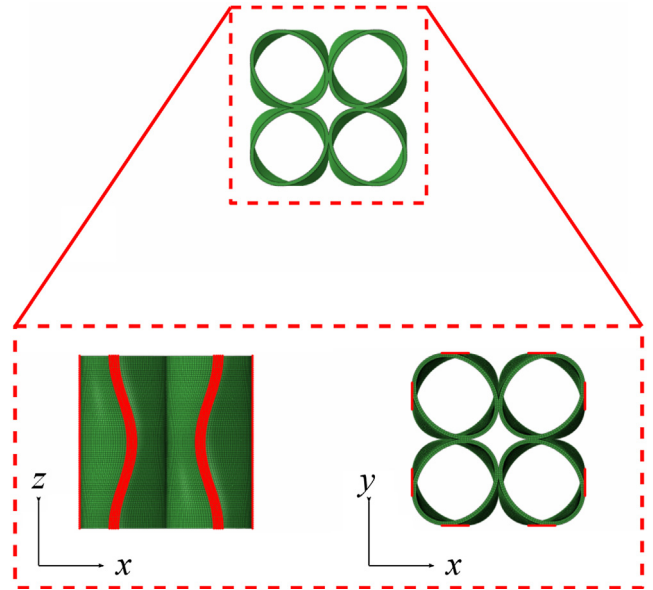

Fig. 6. Location of nodal zero displacement boundary conditions for the honeycomb periodic BC model (upper and lower plates removed for clarity).

Fig. 5. Finite element model of the honeycomb for quasi-static and dynamic conditions.

absorption was defined as the cumulative work done by the structure until densification, as per equation (1).

$$E = \int_0^{\varepsilon_d} \sigma d\varepsilon \tag{1}$$

where σ is the engineering stress, ε is engineering strain and ε_d is the densification strain.

Lastly, energy absorption efficiency (equation (2)), was defined as the ratio of cumulative absorbed energy up to densification strain, divided by the peak stress.

$$\eta = \frac{\int_0^{\varepsilon_d} \sigma d\varepsilon}{\sigma_{peak}} \tag{2}$$

4. Results

4.1. Review of fabricated parts

As illustrated in Fig. 7, honeycomb variants were manufactured through selective laser sintering. Prior to testing, individual mass and dimensions of all specimens (N = 18) were recorded using digital scales and a Vernier Calliper (Absolute AOS Digimatic, Mitutoyo, Japan).

Table A1, located in the appendix, reports individual mass, length, width, depth, and average wall thickness for each sample. Length, width, and depth varied about the design value by only 1.52%, 1.24% and 0.38% respectively, when compared to the CAD models, for all structural variations. For samples with an aspect ratio of e = 1.0, wall thickness exceeded the design value by 38.6%, 27.9% for aspect ratio e = 0.8, and 26.5% variation for e = 0.6.

Visual inspection identified artifacts of the sintering process in certain samples. As highlighted in Fig. 8, samples with an aspect ratio of e = 1.0, had a series of ribs distributed throughout the build axis. At these locations, localised curling [31] has occurred due to a raised area of powder on the build layer. During the following build layer, the raised area limits the deposition of new powder directly on top of the sintered layer, instead being pushed outward causing the rib feature. This feature is not observed in samples with an aspect ratio of e = 0.8 or e = 0.6, because the fold provides a moving cross-sectional area through the z-axis, meaning the material is not sintered normal to the subsequent layer, mitigating the phenomena.
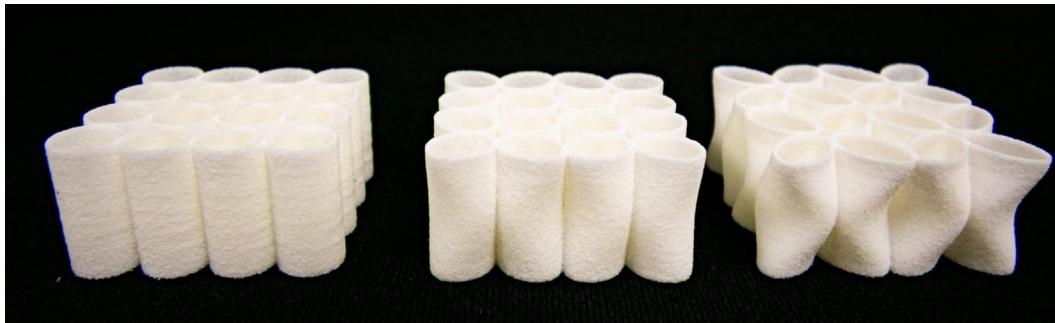

Fig. 7. Fabricated honeycomb samples subject to changing aspect ratio, e = 1.0 (left), e = 0.8 (centre), and e = 0.6 (right).
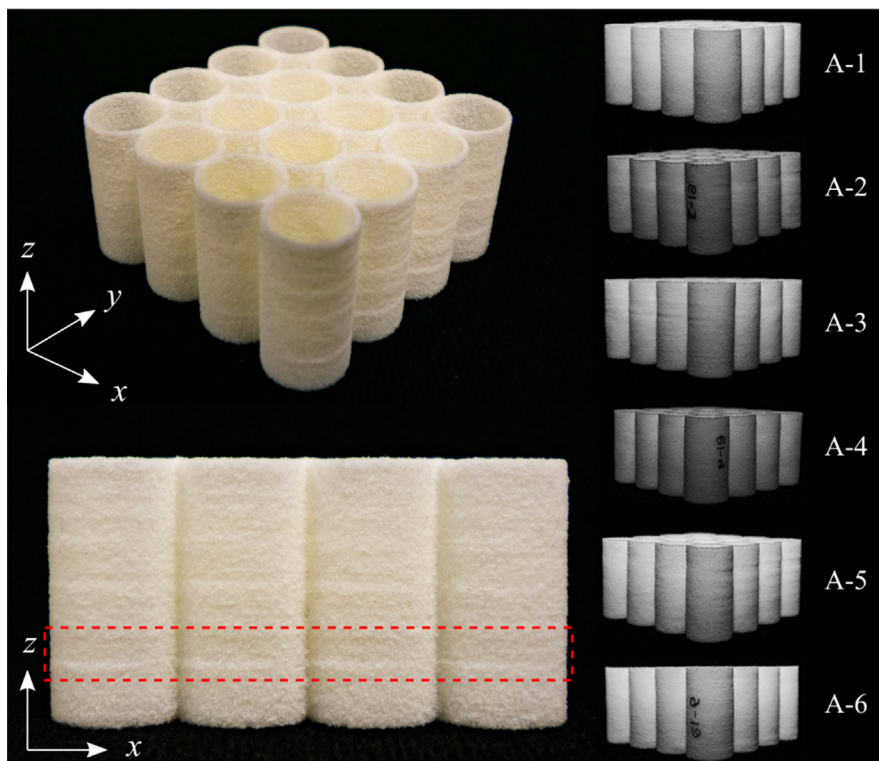

Fig. 8. Identification of sintered rib artifact proliferated through the z-axis height of honeycombs with an aspect ratio of e = 1.0 (straight walled honeycombs).

4.2. Experimental

4.2.1. Quasi-static compression

Quasi-static uniaxial compression was undertaken for each honeycomb variant, with stress–strain curves reported in Fig. 9a–c. For completeness, all data sets (n = 9) for each variant (n = 3) are reported here (See Fig. 10).

For an aspect ratio of e = 1.0, the average yield stress was 0.33 MPa whilst at e = 0.8 and e = 0.6, the average value was 0.24 and 0.18 MPa, respectively (Table 1). For decreasing aspect ratio, the energy absorbed decreases yielding 8.72, 6.20 and 5.17 J respectively. Conversely, the energy absorption efficiency increases to 0.41, 0.43 and 0.46.

4.3. Dynamic compression

Dynamic, free-fall, uniaxial compression was performed for each honeycomb variant, with stress–strain curves reported in Fig. 11a–c. For completeness, all datasets (n = 9) for each variant (n = 3) are reported here. (SEE Fig. 12).

As reported by Table 2, for an aspect ratio e = 1.0, the average yield stress was 0.58 MPa, whilst at e = 0.8 and e = 0.6 the observed yield stress was 0.38 and 0.29 MPa, respectively. In all cases, densification was achieved for the impact, thus enabling calculation of energy absorption efficiency and energy absorbed. In a similar trend to yield stress, values for energy absorbed decreased to 14.69, 10.04 and 8.31 J for decreasing aspect ratio. For energy absorption efficiency the results were 0.41, 0.40, 0.39 for decreasing aspect ratio.

4.4. Rate dependant behaviour

Comparison of the static and dynamic results enables identification of the rate-dependant behaviour. Fig. 13 reports the change in energy absorption with respect to aspect ratio for both the quasi-static and dynamic conditions. The honeycomb structures are sensitive to loading regime. Structures with an aspect ratio of e = 1.0 yield an increase in energy absorption by 69 % between the static and dynamic regime. As the aspect ratio decreases to e = 0.8 and e = 0.6, the associated rate effects increase energy absorption by 62 and 61 % respectively. The relative increase observed between the static and dynamic exceeds that attained for expanded polystyrene (EPS) [32].

The relative increase in yielding stress and energy absorbed is due to the rate dependence of the base material. Previous studies have demonstrated similar phenomena under uniaxial tensile testing whereby a similar relative increase in modulus was observed [30]. The similarity in increase suggests that the rate-dependence observed in this study is due to the base material rate dependence and not structural dependence, such as inertial stabilisation and
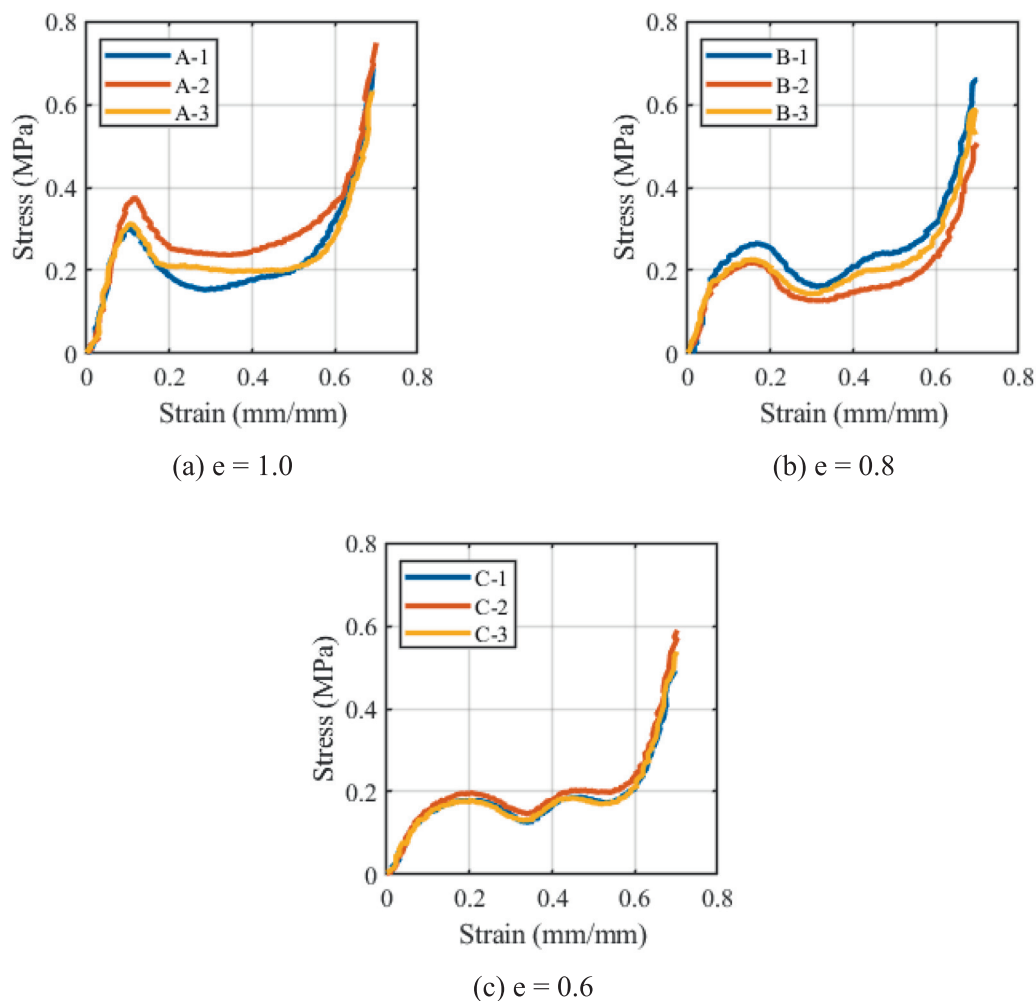

(a) e = 1.0

(b) e = 0.8

(c) e = 0.6

Fig. 9. Engineering stress–strain curves for honeycomb variants subject to changing aspect ratio under quasi-static uniaxial compression.
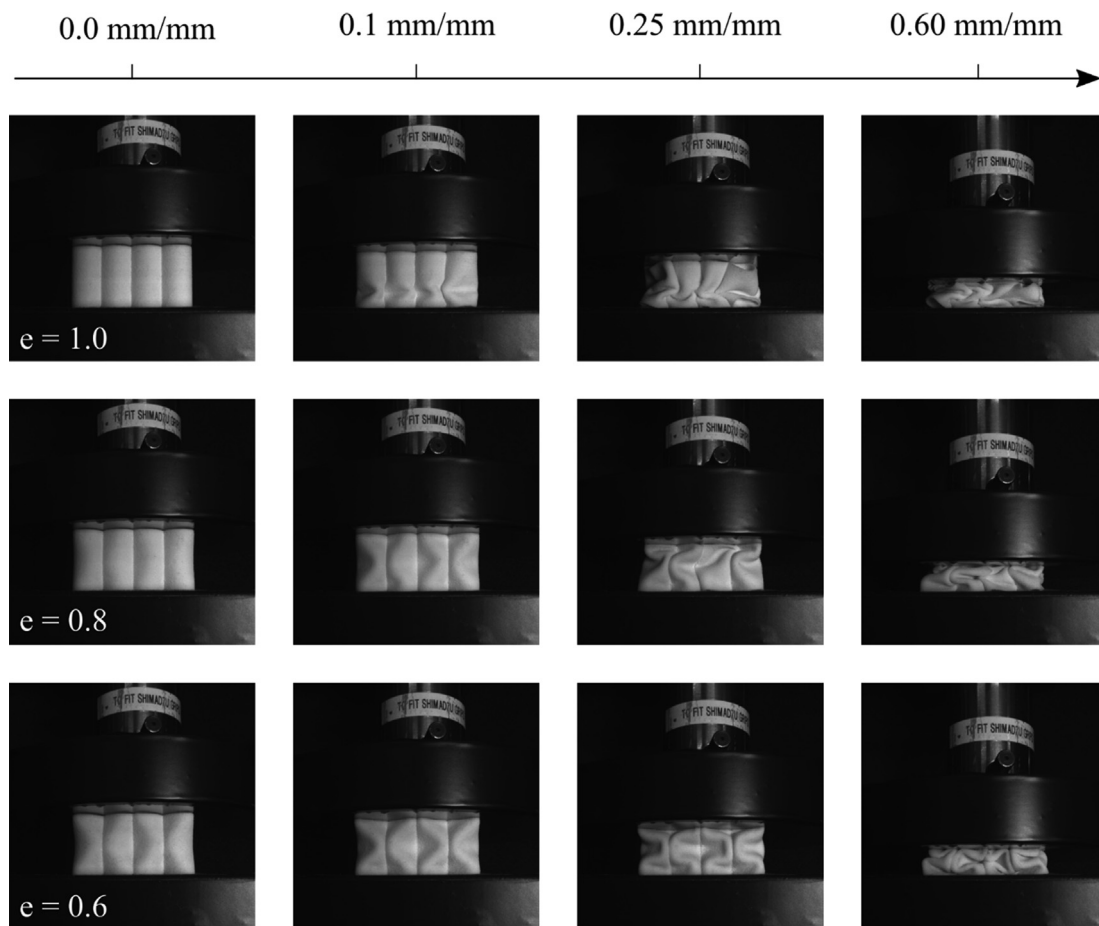
Fig. 10. Photographic stills of the honeycomb samples under quasi-static compression.

Table 1
Average performance parameters yield stress, absorption efficiency and energy absorbed for changing aspect ratio of each honeycomb variant under quasi-static uniaxial compression. Standard deviation in parentheses, CV = coefficient of variation.

	Aspect Ratio	e = 1.0	e = 0.8	e = 0.6
σ_{yield} (MPa)	Mean	0.33 (0.04)	0.24 (0.02)	0.18 (0.01)
	CV (%)	12.08	10.34	5.86
E (J)	Mean	8.72 (1.53)	6.20 (0.53)	5.17 (0.06)
	CV (%)	17.56	8.49	1.12
η	Mean	0.41 (0.03)	0.43 (0.01)	0.46 (0.01)
	CV (%)	6.39	1.07	1.46

plastic wave propagation, which can only be attained at higher strain rates [33].

4.5. Multi-loading behaviour

Following initial tests, each sample was subjected to secondary (1 h after the initial test) and tertiary (24 h after the secondary test) testing under identical conditions, to identify the multiple loading behaviour of the additively manufactured honeycomb structure. Fig. 14a and 14b reports change in energy absorption with respect to aspect ratio for quasi-static and dynamic conditions for each repeat.

For quasi-static conditions, the average energy absorbed was greatest for the virgin compression. A subsequent compression performed an hour later reported a decrease in total energy absorbed of 41, 40 and 35 % for decreasing aspect ratio. The final, tertiary compression occurred 24 h after the secondary test. The calculated energy absorbed during these tests reported a reduc-

tion, when compared to the initial response, of 43, 38 and 30 %. In a similar trend to quasi-static conditions, the calculated energy absorbed under dynamic testing was greatest for the virgin impact. Secondary loading yielded a reduction in total energy absorbed of 31, 21 and 28% for decreasing aspect ratios. The calculated energy absorbed during the tertiary tests reported a reduction, when compared to the initial response, of 27, 28 and 28 %.

Under initial compression, the base material undergoes both elastic and plastic deformation, characterised by base material stress softening and confirmed by the stress reduction in the secondary compressive cycle. During the secondary loading cycle, the base material undergoes exclusively elastic deformation representing a relaxed state. The relaxed state is present in the subsequent compression cycle where the values of yield stress and energy absorbed are consistent with one another. The magnitude of relative decrease in energy absorption, over successive compressive cycles, is markedly greater for quasi-static than dynamic testing. This is attributed to the viscoelastic stress relaxation of the
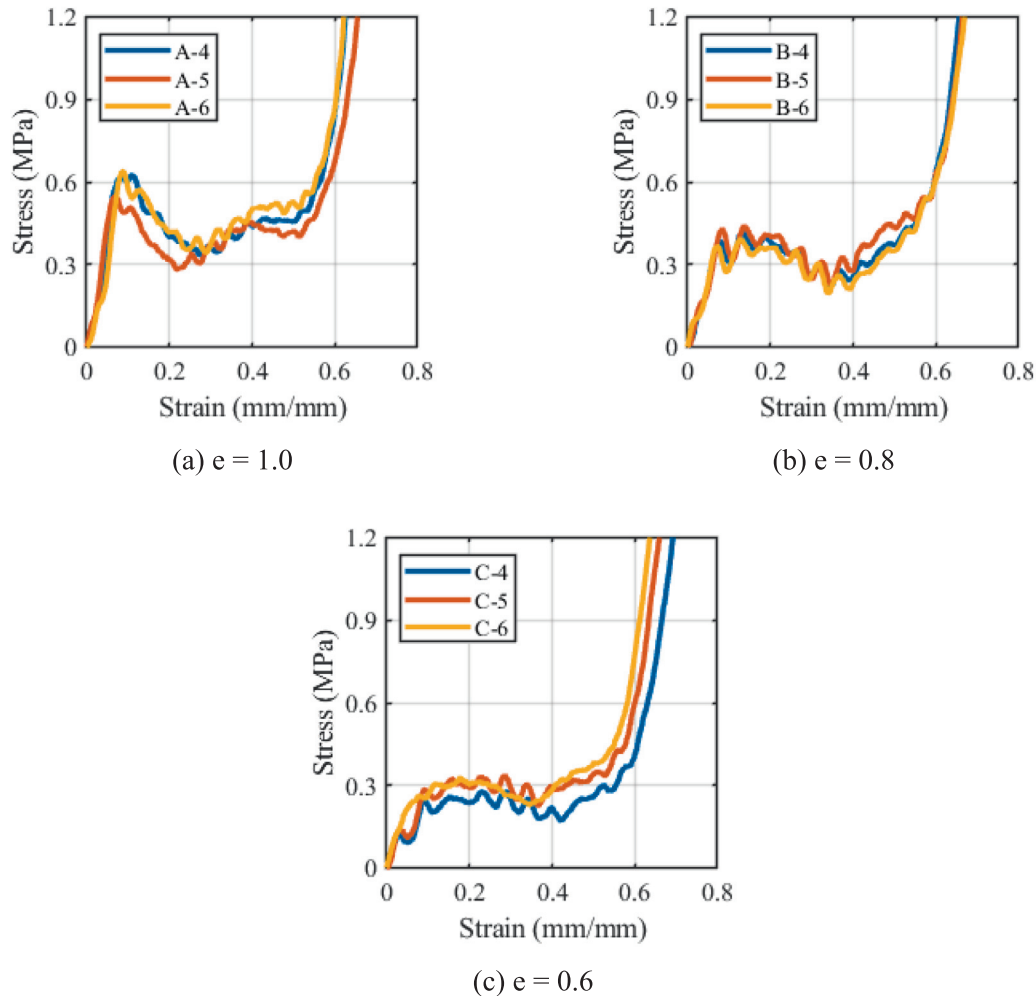
(a) e = 1.0

(b) e = 0.8

(c) e = 0.6

Fig. 11. Engineering stress–strain curves for honeycomb variants subject to changing aspect ratio under dynamic uniaxial compression.

bulk material attaining a greater degree of relaxation. Repeat successive loading was not carried out after 24 h due to a stabilised response. The behaviour reported in this investigation suggests is feasible to achieve a recoverable energy absorbing structure. When sustaining successive, or a history of, impacts this class of materials holds notable advantage over traditional impact mitigating structures. For example, EPS incurs a large degree of plastic deformation over a compression cycle, represented by cracks and permanent set [34,35] that degrades performance when subject to repeat impacts [28].

4.6. Numerical

4.6.1. Quasi-static model

Full-scale and periodic BC model quasi-static simulations were carried out and compared to the collected experimental data, to determine their predictive capacity. The results of both simulations are combined and compared to the experimental data as seen in Fig. 15a–c.

The reduction in CPU run-time, when comparing the full-scale to the periodic BC model, was between 70.39 and 70.63%. Calculated error values for yield stress and energy absorption, when compared to the experimental data, are reported in Table 3. The full model reports good agreement when compared to the experimental data. Generally, the non-linear profile is best represented

for the model with an aspect ratio of e = 1.0, where decreasing aspect ratio yields fair approximation to the stress–strain profile. Yield stress was over- reported by 46.01%, yet the prediction of the total energy absorbed was within 7.50%. For decreasing aspect ratio, the full model error reported for peak stress was between 10.55 and 13.30% and energy absorbed was 0.77–12.28%. The periodic BC model reports fair agreement when compared to the experimental data. For an aspect ratio of e = 1.0, the yield stress was over-reported by 94.17 % and energy absorbed by 31.24 %. For decreasing aspect ratio, the periodic BC model error reported for peak stress is between 19.58 and 27.83% and energy absorbed by 2.14–15.70%.

4.6.2. Dynamic model

Full-scale and periodic BC model dynamic simulations were performed and compared to the collected experimental data to determine their predictive capacity. The results of both simulations are combined and compared to the experimental data as seen in Fig. 16a–c.

The reduction in CPU run-time, when comparing the full-scale to the periodic BC model, was between 75.77 and 76.15%. Calculated error values for yield stress and energy absorption, when compared to the experimental data, are reported in Table 4. The full-scale finite element models report good agreement when compared to the experimental data. Generally, the non-linear profile is
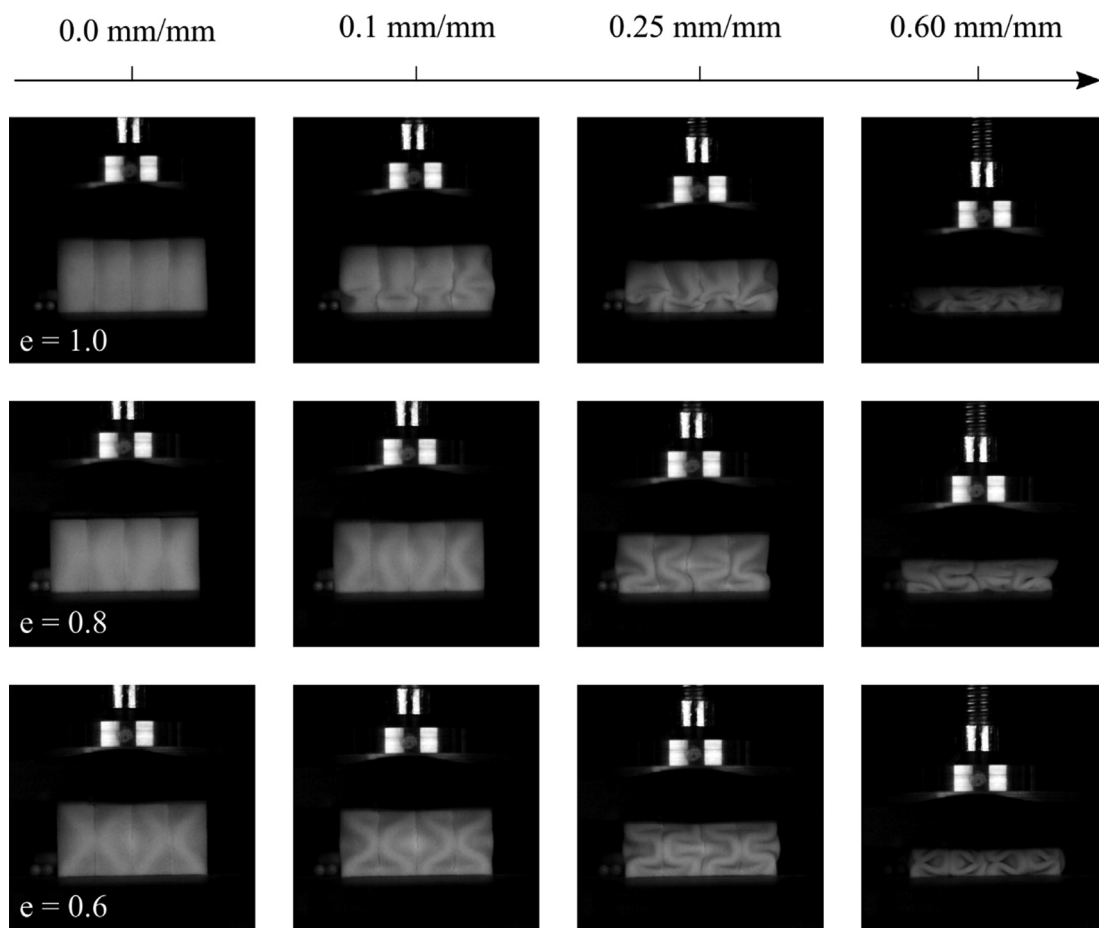
Fig. 12. Photographic stills of the honeycomb samples under dynamic compression.

Table 2
Average performance parameters yield stress, absorption efficiency and energy absorbed for changing aspect ratio of each honeycomb variant under dynamic uniaxial compression. Standard deviation in parentheses, CV = coefficient of variation.

	Aspect Ratio	e = 1.0	e = 0.8	e = 0.6
σ_{yield} (MPa)	Mean	0.58 (0.05)	0.38 (0.02)	0.29 (0.04)
	CV (%)	8.66	5.42	12.37
E (J)	Mean	14.69 (0.90)	10.04 (1.39)	8.31 (0.92)
	CV (%)	6.15	13.81	11.03
η	Mean	0.41 (0.01)	0.40 (0.01)	0.39 (0.02)
	CV (%)	2.95	2.06	4.40

well represented for all models. In a similar trend to the quasi-static full model, the yield stress was over reported by 48.70%, whilst the prediction of energy absorbed was within 23.56%. For decreasing aspect ratio, the error reported for peak stress was between 0.36 and 1.91% and energy absorbed was 2.86–6.29%.

The periodic BC model also achieved good agreement with the experimental data, except for the structure with an aspect ratio of e = 1.0, where yield stress was over-reported by 93.36% and energy absorption by 62.01%. For decreasing aspect ratio, the periodic BC model error reported for yield stress was between 17.40–26.5% and 11.94–25.50% for energy absorption.

4.6.3. Parameter sweep

To understand the relationship between the aspect ratio and wall thickness under dynamic conditions, the periodic BC model under constant strain rate conditions was leveraged to undertake a full factorial parameter sweep. This approach combined the quasi-static modelling, dynamic material properties and a constant

strain rate equivalent to the previous impact loading. This approach was adopted such that each simulation achieved densification, enabling calculation of energy absorption and absorption efficiency. The validity of adopting this approach compared to impact loading was assessed and did not yield a notable difference. Yield stress, energy absorption and efficiency were calculated for each simulated response. The results were assembled into contour plots as illustrated in Fig. 17a–c. The overlaid black crosses indicate each simulation point. Energy absorption and efficiency were calculated up to densification strain.

Fig. 17a–b exhibit similar trends, where yield stress and energy absorbed increase towards the right-hand corner of the plot. Values reported range from 0.37–11.82 MPa and 10.20–222.0 J respectively, representing an increase in several orders of magnitude. The area of maxima corresponds to a traditional honeycomb, e.g., wall thickness, t = 2.2 mm, and aspect ratio, e = 1.0. Fig. 17c reports a range of energy absorption efficiency between 0.30 and 0.45. Unlike Fig. 17a and 17b, a broad region of maximum values
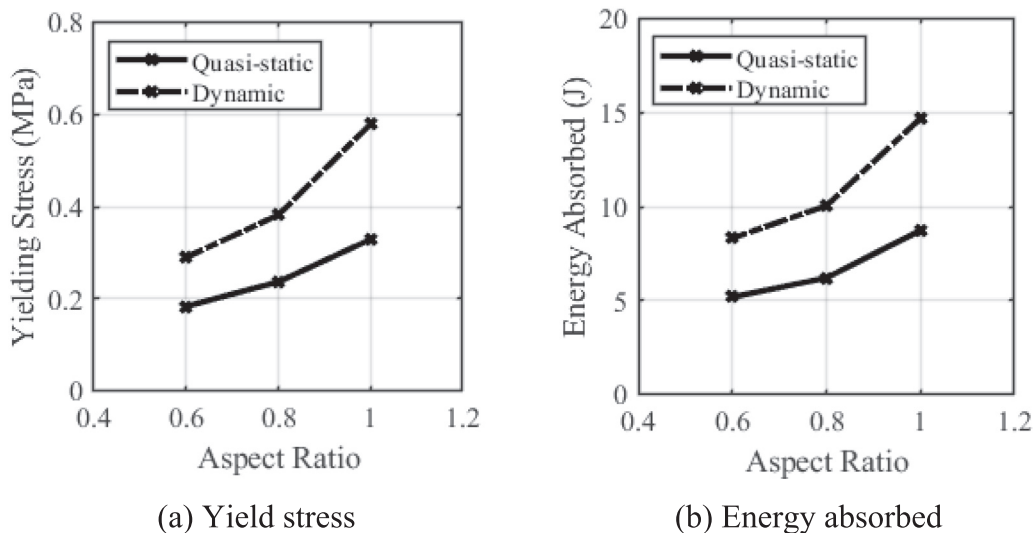
(a) Yield stress

(b) Energy absorbed

Fig. 13. Comparison of strain rate behaviour for quasi-static and dynamic uniaxial compression.

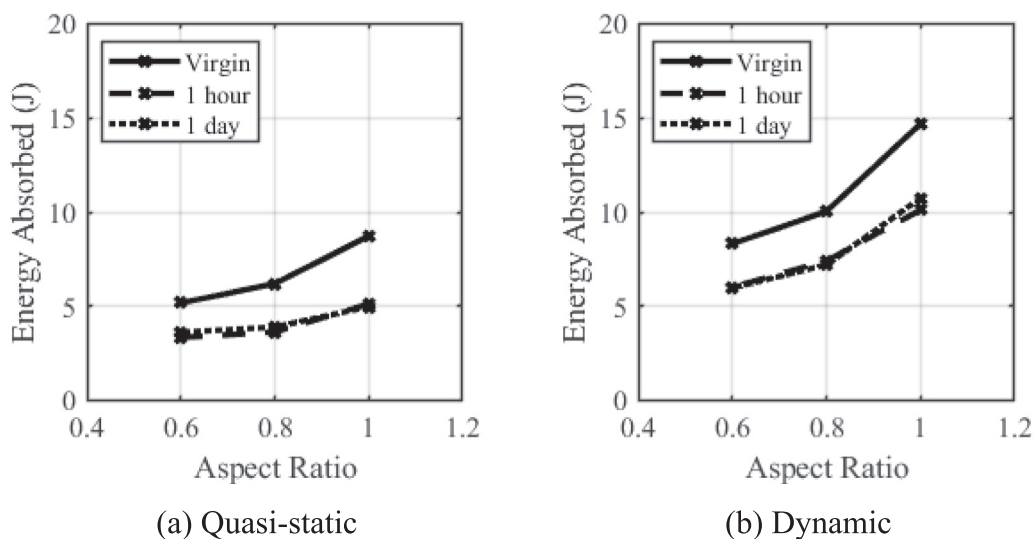
(a) Quasi-static

(b) Dynamic

Fig. 14. Comparison of multi-loading energy absorbed under quasi-static and dynamic uniaxial compression.

is observed and positioned in the lower left-hand region. This region of maximum values corresponds to a honeycomb of varying structure and is defined by values of wall thickness, t = 0.6–1.2 mm, and aspect ratio, e = 0.6–0.9.

5. Discussion

This study aimed to investigate the mechanical behaviour and energy absorption ability of various geometric configurations of a circular, pre-buckled honeycomb. This paper's rationale is informed by [26]. It extends the analysis to include dynamic compressive behaviour, whilst leveraging periodic BC models to interrogate the design space and provide a foundation for optimising these structures for future design applications, based on specific loading regimes and acceptable performance parameter thresholds.

When axially compressed, the honeycomb samples demonstrated various mechanical behaviours. For an aspect ratio e = 1.0, typical honeycomb behaviour is observed where there is an initial linear response. Continued strain introduces stress nonlinearity. Buckling occurs once the walls of the honeycomb cells are axially deformed beyond a critical yield point. The period of buckling is associated with stress softening. In contrast to metallic, polymeric, or paper honeycombs, honeycombs derived from elastomeric materials present softening for a greater period of compression [36]. The onset of buckling reduces the stiffness of the structure; however, the failure mechanism is characterised by bending of the cell walls rather than folding at plastic boundaries. Consequently, the non-linear region of buckling is more pronounced, and the plateau region is diminished. In contrast, the introduction of an aspect ratio less than 1.0 yields atypical honeycomb behaviour, achieving a reduction in yield stress and prolongation of the non-linear buckling region. Moreover, characteristic stress softening, which is a limiting factor of traditional honey-
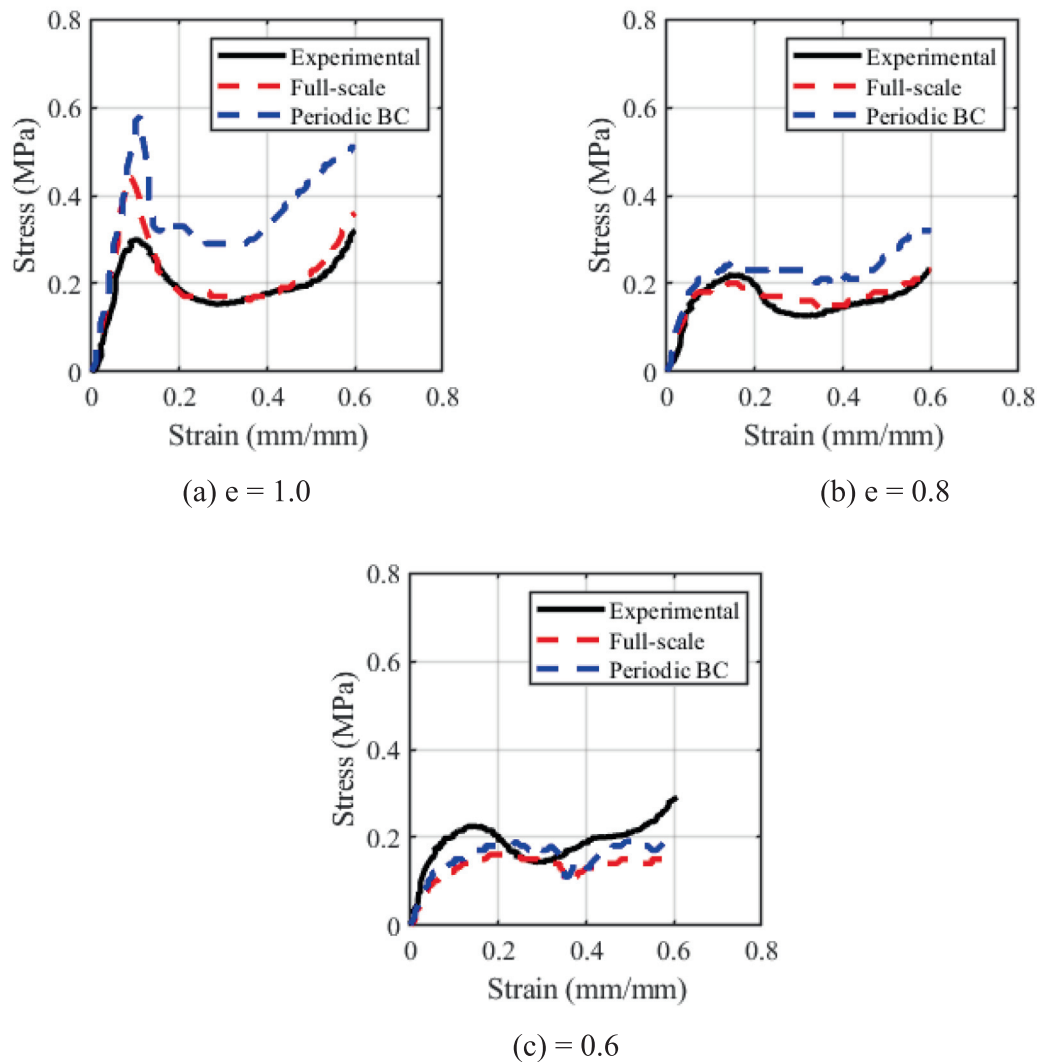
(a) e = 1.0

(b) e = 0.8

(c) = 0.6

Fig. 15. Comparison of the experimental quasi-static compression mechanical behaviour to the full simulation and periodic BC model result for various aspect ratios.

Table 3
Computed performance parameter (yield stress and energy absorbed) error when compared to experimental data for quasi-static uniaxial compression full and periodic BC model.

e	Model	$\sigma_{yield, er}$ (%)	E_{er}(%)
1.0	Full	46.01	7.38
	Periodic BC	94.17	31.24
0.80	Full	10.55	12.28
	Periodic BC	19.58	2.14
0.60	Full	13.30	0.77
	Periodic BC	27.83	15.70

combs, is less prominent. As the aspect ratio is decreased, the buckling mode becomes more controlled as axial crushing is guided by the introduction of the fold. The overall response tends towards a square shape, mimicking the response seen in conventional polymeric foams and achieving an improvement in energy absorption efficiency [1].

Variability in the quasi-static response was identified through the examination of standard deviation and coefficient of variation. The variance observed is attributed to the prominence of slipping at the upper and lower faces, which changes the characteristic response of the structure. This is most notable with structures that

have an aspect ratio of e = 1.0. The prevalence of slipping is due to a lateral force that develops as each cell buckles, overcoming the friction at the upper and lower face. As the aspect ratio decreases, the introduction of the fold facilitates a reduction in the lateral force and therefore preserves the true response of the honeycomb. Values of standard deviation and coefficient of variation in dynamic testing suggest the prevalence of a lateral force overcoming friction at the impact interface is less significant. Previous authors have utilised design modifications such as a solid boss at the upper and lower face, constrained by adhesive tape at the platen [37]. This restraint isolates the buckling response of the honeycombs; however, it was not achievable in this present investigation as it would trap a volume of un-sintered powder.

Full scale and periodic BC finite element models were developed to represent the experimental setup. Greater comparability was obtained for energy absorbed than was for yield stress. Failure to accurately predict the yield stress is associated with the prevalence of fault lines throughout the mid-section of the honeycomb structure due to curling (refer to Fig. 8). The prevalence of this feature is endemic in sintering thin wall structures [38] and presents a challenge to model computationally. Including this feature within the model would have been infeasible due to the reduction in mesh size required to attain such a feature, necessitating significantly
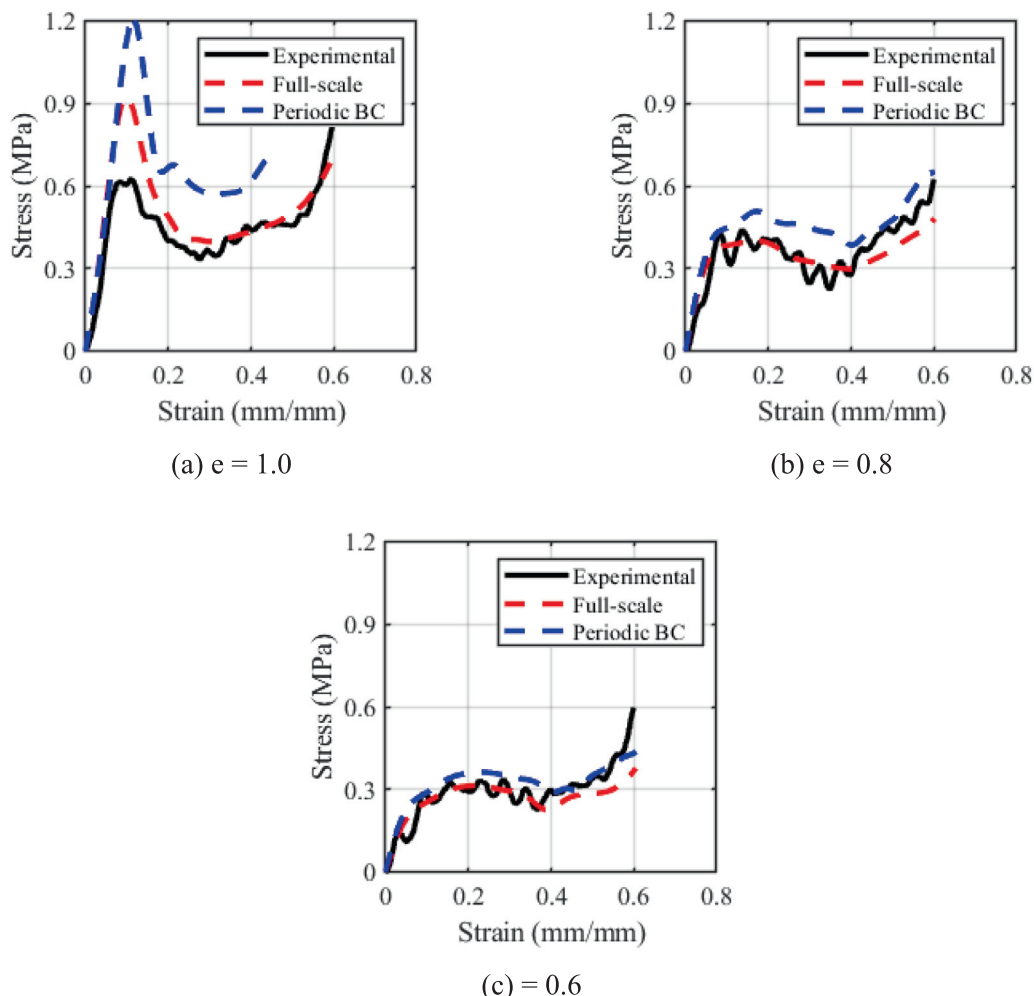
(a) e = 1.0

(b) e = 0.8

(c) = 0.6

Fig. 16. Comparison of the experimental dynamic compression mechanical behaviour to the full simulation and periodic BC model for various aspect ratios.

Table 4
Computed performance parameter (yield stress and energy absorbed) error when compared to experimental data for dynamic uniaxial compression full and periodic BC model.

e	Model	$\sigma_{yield, er}$ (%)	E_{er}(%)
1.0*	Full	48.70	23.56
	Periodic BC	94.36	62.01
0.80	Full	0.36	2.86
	Periodic BC	26.5	25.5
0.60	Full	1.91	6.29
	Periodic BC	17.40	11.94

* For the case of e = 1.0, analysis was limited to ε = 0.4 mm/mm because the periodic BC model simulation did not yield densification.

greater computational cost. Future studies should investigate and model imperfections that arise due to additive manufacture of thin-walled structure. Furthermore, the validated periodic BC finite element models represent an efficient route to investigate the interplay between the previously investigated geometric parameters and other (e.g. cell size and number of folds).

6. Conclusions

In this paper, various configurations of pre-buckled circular honeycomb were designed and fabricated using an elastomeric

powder and the laser sintering method. The mechanical behaviour of the additively manufactured pre-buckled honeycombs was investigated under quasi-static and dynamic compression both experimentally and numerical. The main conclusions are:

1. Tailorable mechanical behaviour was observed subject to changing the pre-buckle design feature aspect ratio whilst maintaining wall thickness.
2. Notable rate-dependant behaviour was observed when comparing quasi-static and dynamic conditions. The relative increase in energy absorption exceeds that of traditional polymeric foam.
3. Stabilised multi-loading behaviour was observed after successive loading cycles. The material and structural configuration offers good potential for repeat impact mitigating applications.
4. The full-scale finite element model accurately predicts the mechanical response of elastomeric honeycomb under quasi-static and dynamic compression.
5. The periodic BC finite element model accurately predicts the mechanical response of elastomeric honeycomb under quasi-static and dynamic compression.
6. Parameter sweeps of the periodic boundary condition FE model identified a broad range of dynamic mechanical behaviour, providing a foundation for optimising this structure subject to application specific loading regimes and acceptable performance thresholds.
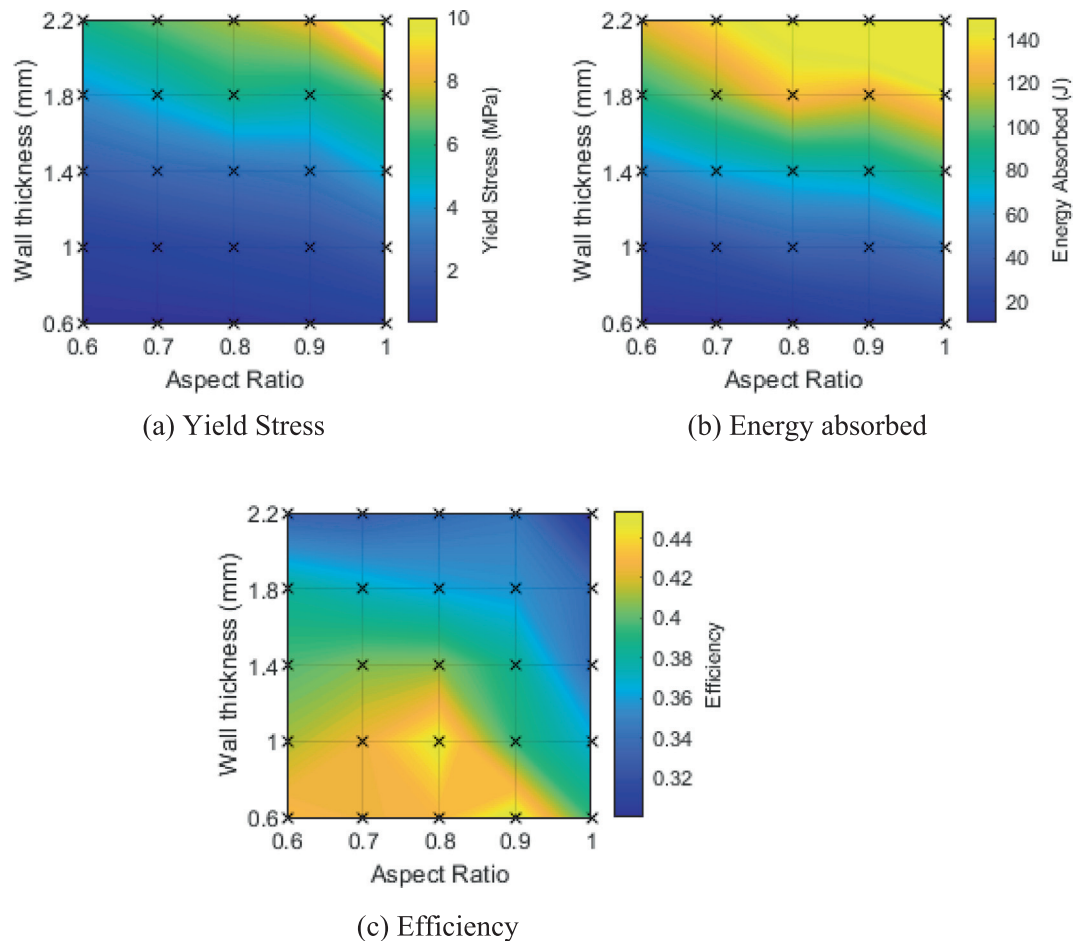
(a) Yield Stress

(b) Energy absorbed

(c) Efficiency

Fig. 17. Variation in dynamic honeycomb mechanical behaviour relative to changing wall thickness and aspect ratio.

Declaration of Competing Interest

The authors declare that they have no known competing financial interests or personal relationships that could have appeared to influence the work reported in this paper.

Acknowledgements

Appendix A. Supplementary material

Supplementary data to this article can be found online at https://doi.org/10.1016/j.matdes.2021.110368.

References

[1] L.J. Gibson, M.F. Ashby, Cellular solids: Structure and properties, 2nd ed., Cambridge University Press, 2014.
[2] Z. Wang, Recent advances in novel metallic honeycomb structure, Compos. B Eng. 166 (2019) 731–741.
[3] J.M. Jafferson, S. Pattanashetti, Use of 3D printing in production of personal protective equipment (PPE) - a review, Mater. Today Proc. 46 (2021) 1247–1260.
[4] Y. Chen, T. Li, Z. Jia, F. Scarpa, C.-W. Yao, L. Wang, 3D printed hierarchical honeycombs with shape integrity under large compressive deformations, Mater. Des. 137 (2018) 226–234.
[5] K.M. Rahman, Z. Hu, T. Letcher, In-Plane stiffness of additively manufactured hierarchical honeycomb metamaterials with defects, J. Manuf. Sci. Eng. Trans. ASME 140 (1) (2018).

[6] A. Ajdari, H. Nayeb-Hashemi, A. Vaziri, Dynamic crushing and energy absorption of regular, irregular and functionally graded cellular structures, Int. J. Solids Struct. 48 (3-4) (2011) 506–516.
[7] O. Rahman, B. Koohbor, Optimization of energy absorption performance of polymer honeycombs by density gradation, Compos. Part C Open Access 3 (2020) 100052.
[8] J.A. Harris, G.J. McShane, Impact response of metallic stacked origami cellular materials, Int. J. Impact Eng. 147 (2021) 103730.
[9] J.A. Harris, G.J. McShane, Metallic stacked origami cellular materials: Additive manufacturing, properties, and modelling, Int. J. Solids Struct. 185-186 (2020) 448–466.
[10] Z. Zhao et al., 3D printing of complex origami assemblages for reconfigurable structures, Soft Matter 14 (39) (2018) 8051–8059.
[11] J. Qi, C. Li, Y. Tie, Y. Zheng, Y. Duan, Energy absorption characteristics of origami-inspired honeycomb sandwich structures under low-velocity impact loading, Mater. Des. 207 (2021) 109837.
[12] W. Jabi, S. Soe, P. Theobald, R. Aish, S. Lannon, Enhancing parametric design through non-manifold topology, Des. Stud. 52 (2017) 96–114.
[13] J. Wang, R. Rai, International Journal of Production Research Generative design of conformal cubic periodic cellular structures using a surrogate model-based optimisation scheme Generative design of conformal cubic periodic cellular structures using a surrogate model-based optimisation scheme, 2020.
[14] S. Antony, A. Cherouat, G. Montay, Fabrication and characterization of hemp fibre based 3D printed honeycomb sandwich structure by FDM process, Appl. Compos. Mater. 27 (6) (2020) 935–953.
[15] C. Quan, B. Han, Z. Hou, Q. Zhang, X. Tian, T.J. Lu, 3d printed continuous fiber reinforced composite auxetic honeycomb structures, Compos. Part B Eng. 187 (2020) 107858.
[16] Y. Zhang, T. Liu, H. Ren, I. Maskery, I. Ashcroft, Dynamic compressive response of additively manufactured AlSi10Mg alloy hierarchical honeycomb structures, Compos. Struct. 195 (2018) 45–59.
[17] J.A. Harris, R.E. Winter, G.J. McShane, Impact response of additively manufactured metallic hybrid lattice materials, Int. J. Impact Eng. 104 (2017) 177–191.
[18] R. Hedayati, M. Sadighi, M. Mohammadi-Aghdam, A.A. Zadpoor, Mechanical properties of additively manufactured octagonal honeycombs, Mater. Sci. Eng. C 69 (2016) 1307–1317.

[19] F.N. Habib, P. Iovenitti, S.H. Masood, M. Nikzad, In-plane energy absorption evaluation of 3D printed polymeric honeycombs, Virtual Phys. Prototyp. 12 (2) (2017) 117–131.

[20] Y. Kim, M.M. Tentzeris, S. Lim, Low-loss and light substrate integrated waveguide using 3D printed honeycomb structure, Materials (Basel) 12 (3) (2019) 402.

[21] D. Chen, X. Zheng, Multi-material additive manufacturing of metamaterials with giant, tailorable negative poisson's ratios, Sci. Rep. 8 (1) (2018) 9139.

[22] M. Bodaghi, A. Serjouei, A. Zolfagharian, M. Fotouhi, H. Rahman, D. Durand, Reversible energy absorbing meta-sandwiches by FDM 4D printing, Int. J. Mech. Sci., vol. 173, no. September 2019, p. 105451, 2020.

[23] S.R.G. Bates, I.R. Farrow, R.S. Trask, 3D printed polyurethane honeycombs for repeated tailored energy absorption, Mater. Des. 112 (2016) 172–183.

[24] S.R.G. Bates, I.R. Farrow, R.S. Trask, Compressive behaviour of 3D printed thermoplastic polyurethane honeycombs with graded densities, Mater. Des. 162 (2019) 130–142.

[25] J.H. Park, J.R. Lee, Developing fall-impact protection pad with 3D mesh curved surface structure using 3D printing technology, Polymers (Basel) 11 (11) (2019) 1800.

[26] S. Townsend, R. Adams, M. Robinson, B. Hanna, P. Theobald, 3D printed origami honeycombs with tailored out-of-plane energy absorption behavior, Mater. Des. 195 (2020) 108930.

[27] T. Whyte et al., A review of impact testing methods for headgear in sports: considerations for improved prevention of head injury through research and standards, J. Biomech. Eng. 141 (2019) 70803–70804.

[28] C.G. Mattacola, C. Quintana, J. Crots, K.I. Tumlin, S. Bonin, Repeated impacts diminish the impact performance of equestrian helmets, J. Sport Rehabil. 28 (4) (2019) 368–372.

[29] "Friction and Friction Coefficients." [Online]. Available: https://www. engineeringtoolbox.com/friction-coefficients-d_778.html. [Accessed: 07-Jun-2021].

[30] R. Adams et al., A novel pathway for efficient characterisation of additively manufactured thermoplastic elastomers, Mater. Des. 180 (2019) 107917.

[31] S.P. Soe, Quantitative analysis on SLS part curling using EOS P700 machine, J. Mater. Process. Technol. 212 (11) (2012) 2433–2442.

[32] N.J. Mills, S. Wilkes, S. Derler, A. Flisch, FEA of oblique impact tests on a motorcycle helmet, Int. J. Impact Eng. 36 (7) (2009) 913–925.

[33] Y. Zhang, T. Liu, W. Tizani, Experimental and numerical analysis of dynamic compressive response of Nomex honeycombs, Compos. Part B Eng. 148 (2018) 27–39.

[34] C. Ling, J. Ivens, P. Cardiff, M.D. Gilchrist, Deformation response of EPS foam under combined compression-shear loading. Part I: Experimental design and quasi-static tests, Int. J. Mech. Sci. 144 (2018) 480–489.

[35] C. Ling, J. Ivens, P. Cardiff, M.D. Gilchrist, Deformation response of EPS foam under combined compression-shear loading. Part II: High strain rate dynamic tests, Int. J. Mech. Sci. 145 (2018) 9–23.

[36] T. Thomas, G. Tiwari, Crushing behavior of honeycomb structure: a review, Int. J. Crashworthiness 24 (5) (2019) 555–579.

[37] M. Robinson, S. Soe, R. Johnston, R. Adams, B. Hanna, R. Burek, G. McShane, R. Celeghini, M. Alves, P. Theobald, Mechanical characterisation of additively manufactured elastomeric structures for variable strain rate applications, Addit. Manuf. 27 (2019) 398–407.

[38] S.P. Soe, D.R. Eyers, R. Setchi, Assessment of non-uniform shrinkage in the laser sintering of polymer materials, Int. J. Adv. Manuf. Technol. 68 (1-4) (2013) 111–125.